AMERICAN SOCIETY FOR MICROBIOLOGY | mSphere®

RESEARCH ARTICLE

Both *Pseudomonas aeruginosa* and *Candida albicans* Accumulate Greater Biomass in Dual-Species Biofilms under Flow

Swetha Kasetty,[a] Dallas L. Mould,[b] Deborah A. Hogan,[b] Carey D. Nadell[a]

[a]Department of Biological Sciences, Dartmouth, Hanover, New Hampshire, USA
[b]Department of Microbiology and Immunology, Geisel School of Medicine at Dartmouth, Hanover, New Hampshire, USA

ABSTRACT Microbe-microbe interactions can strongly influence growth and biofilm formation kinetics. For *Pseudomonas aeruginosa* and *Candida albicans*, which are found together in diverse clinical sites, including urinary and intravenous catheters and the lungs of individuals with cystic fibrosis (CF), we compared the kinetics of biofilm formation by each species in dual-species and single-species biofilms. We engineered fluorescent protein constructs for *P. aeruginosa* (producing *mKO-κ*) and *C. albicans* (producing *mKate2*) that did not alter growth and enabled single-cell resolution imaging by live-sample microscopy. Using these strains in an optically clear derivative of synthetic CF sputum medium, we found that both *P. aeruginosa* and *C. albicans* displayed increased biovolume accumulation—by three- and sixfold, respectively—in dual-species biofilms relative to single-species biofilms. This result was specific to the biofilm environment, as enhanced growth was not observed in planktonic cocultures. Stimulation of *C. albicans* biofilm formation occurred regardless of whether *P. aeruginosa* was added at the time of fungal inoculation or 24 h after the initiation of biofilm development. *P. aeruginosa* biofilm increases in cocultures did not require the Pel extracellular polysaccharide, phenazines, and siderophores known to influence *C. albicans*. *P. aeruginosa* mutants lacking Anr, LasR, and BapA were not significantly stimulated by *C. albicans*, but they still promoted a significant enhancement of biofilm development of the fungus, suggesting a fungal response to the presence of bacteria. Last, we showed that a set of *P. aeruginosa* clinical isolates also prompted an increase of biovolume by *C. albicans* in coculture.

IMPORTANCE There is an abundance of work on both *P. aeruginosa* and *C. albicans* in isolation, and quite some work as well on the way these two microbes interact. These studies do not, however, consider biofilm environments under flow, and our results here show that the expected outcome of interaction between these two pathogens can actually be reversed under flow, from pure antagonism to an increase in biomass on the part of both. Our work also highlights the importance of cellular-scale spatial structure in biofilms for understanding multispecies population dynamics.

KEYWORDS *Candida albicans*, *Pseudomonas aeruginosa*, artificial sputum, biofilm, confocal microscopy, cystic fibrosis, flow, image analysis, microfluidics, population dynamics, spatial ecology

Microbial biofilm growth, even in monospecies contexts, involves the interplay of many biological and physical factors that are dynamic in space and time (1–3). In many natural environments, including numerous chronic infections, biofilms are multispecies mixtures whose collective properties and dynamics may be difficult to predict from those of each constituent's monospecies biofilm growth. In the context of infection, the extent and kind of interactions among different biofilm-dwelling microbes also govern clinically relevant factors, such as drug resistance and virulence (4). For

Citation Kasetty S, Mould DL, Hogan DA, Nadell CD. 2021. Both *Pseudomonas aeruginosa* and *Candida albicans* accumulate greater biomass in dual-species biofilms under flow. mSphere 6:e00416-21. https://doi.org/10.1128/mSphere.00416-21.

Editor Aaron P. Mitchell, University of Georgia

Address correspondence to Carey D. Nadell, carey.d.nadell@dartmouth.edu.

Received 3 May 2021
Accepted 5 May 2021
Published 23 June 2021

example, multispecies biofilm growth has been implicated in conjunctivitis (5), tooth decay (6), prosthesis and wound infections (7, 8), and respiratory diseases (9, 10). Clinical microbiologists are just starting to consider the multispecies nature of pathogenic biofilms and its implications for prevention and treatment (11).

Exemplars of chronic, multispecies biofilm infections are those that occur consistently in the lungs of patients with cystic fibrosis (CF), a genetic disorder in humans as a result of mutations in the cystic fibrosis transmembrane conductance regulator. Disruption of this protein's function results in pathologies throughout the body including the accumulation of highly viscous mucus in the lungs, which hinders normal mucociliary clearance. As a result, bacterial and fungal pathogens that would otherwise be easily removed from healthy lungs instead accumulate and lead to chronic infections (12). Chronic CF lung infections are caused by diverse and metabolically flexible populations and consortia, and they are extremely recalcitrant to antibiotic and phagocytic clearance (13). While the ecology of the infecting species shapes the community and potentially has a profound influence on disease severity in the CF lung, it remains poorly understood (9). Given that the spatial interactions of pathogens can strongly affect disease outcome (14), we aimed to create an experimental model *in vitro* to investigate the biofilm formation kinetics of one or more species in coculture. Studies of multispecies biofilm formation and biofilm dynamics in general benefit tremendously from high-resolution imaging, which allows for studying the cell-length-scale behaviors and higher-order structures that contribute to the community's cumulative growth, organization, and function. However, imaging live biofilms *in situ* is often difficult, if not impossible, in many natural contexts. A helpful strategy to mitigate this problem is to reconstitute key features of the *in situ* environment using an *in vitro* system that is more amenable to imaging.

Here, we chose to study *Pseudomonas aeruginosa* and *Candida albicans* as representatives of potentially interacting species in a polymicrobial CF infection, as both these species are commonly isolated from CF lung infections and believed to be important copathogens in patients (15). They are also thought to cooccur in other infection environments, including trauma wounds and surrounding urinary catheters (16). *C. albicans* is a polymorphic and opportunistic pathogen with the ability to form invasive hyphal filaments and drug-resistant biofilms (17). *P. aeruginosa* is another opportunistic pathogen with diverse virulence mechanisms, to which biofilm formation contributes directly and indirectly (18). *P. aeruginosa-C. albicans* interactions are well studied in liquid and agar colony models. Among the primary findings from this literature, *P. aeruginosa* has been shown to preferentially attach to and form biofilms on *C. albicans* hyphae in static culture, eventually killing them (19), but *P. aeruginosa* also inhibits the yeast-to-hyphal switch of *C. albicans* in liquid and agar colony cultures, enhancing *C. albicans* survival (20). Prior work has intimated a feedback loop whereby *C. albicans* produces ethanol, which increases biofilm formation, inhibits swarming motility, and enhances the production of antifungal phenazines on the part of *P. aeruginosa* (21, 22). These phenotypes in turn cause downregulation of the central pathway that induces hyphal growth and inhibit mitochondrial activity, stimulating further ethanol production by *C. albicans* (23). On the other hand, some *in vivo* experiments using a zebrafish model have indicated mutually enhanced virulence of the two species, suggesting that environmental shifts may have strong impacts on the properties of cocultures of these microbes (24). As local concentrations of metabolic products involved in interspecies interactions are determined by the relative and absolute abundances, it is critical to understand the dynamics of biofilm formation for each species in mixed culture.

Using engineered strains with novel fluorescent protein constructs and microfluidic culture with a modified synthetic sputum medium allowing for high-resolution imaging of *C. albicans* and *P. aeruginosa*, we show that their biofilm architecture, rates of biovolume accumulation, and total biovolume is higher for each species in coculture versus monococulture. Growth stimulation for either species was not observed in planktonic coculture conditions. This result is robust to different clinical strains of

P. aeruginosa and a variety of deletion mutants lacking factors known to participate in *P. aeruginosa-C. albicans* interactions.

RESULTS

Biofilm profiles in mono- and dual-species culture. We aimed to characterize the architecture of monospecies and dual-species biofilms of *P. aeruginosa* and *C. albicans* under flow in a medium that represents the chemical composition of CF sputum. Synthetic cystic fibrosis medium (SCFM2), developed and refined by the Whiteley group (25, 26), is a field standard for this purpose, but this medium is not optically clear due to the presence of reconstituted mucins. To generate an optically clear medium for imaging—and supported by data showing that *P. aeruginosa* does not degrade mucins itself (27)—we made a modified version of SCFM in which the major mucin glycans were substituted for mucin; we term this modified medium artificial sputum medium for imaging, or ASMi (see Materials and Methods). Each species' growth profile was the same SCFM2 as it was in ASMi (see Fig. S1 in the supplemental material).

P. aeruginosa and *C. albicans* were modified by allelic exchange to contain a chromosomal construct for constitutive expression of tandem, codon-optimized copies of *mKO-κ* (*P. aeruginosa*) or a single copy of *mKate2* (*C. albicans*) (see Materials and Methods). *mKO-κ* or *mKate2* was selected for these studies for their brightness and because they could be easily distinguished by fluorescence microscopy. The fluorescent protein expression constructs did not alter the growth rate of either species (Fig. S2).

To investigate mono- and dual-culture biofilm growth under flow of ASMi, we inoculated derivatives of *P. aeruginosa* strain PA14 and *C. albicans* strains CAI4 either alone or together in microfluidic devices (see Materials and Methods). Monoculture *P. aeruginosa* chambers contained small biofilms with compact microcolonies on the order of 10 μm in height (Fig. 1A). Monoculture biofilms of *C. albicans* contained scattered clusters of groups of elongated yeast, many pseudohyphae, and some true hyphae that spanned the height of the chamber (Fig. 1B). By visual inspection of confocal images, it was quickly clear that the architecture and total accumulation of both species were quite different in dual-inoculated conditions compared to the monoculture biofilms. In coculture, *C. albicans* had largely formed true hyphae (Fig. 1C). Quantification of *C. albicans* biovolume found a higher biovolume density near the base of the biofilm in coculture conditions (Fig. 1D). In coculture, *P. aeruginosa* biofilms localized to the hyphae of the highly filamentous *C. albicans* biofilms (Fig. 1C). The biovolume accumulation of *P. aeruginosa* in coculture appeared greater, particularly in the regions also colonized by *C. albicans* (0 to 12 μm from the glass substratum) (Fig. 1D).

Quantitative analysis of image stacks from replicate biofilms collected from independent experiments found that the total biovolume of both species increased substantially in coculture relative to monoculture (Fig. 2A and B). The increase in biofilm biovolume in coculture was significant by 24 h for *C. albicans* (Fig. 2A) and for *P. aeruginosa* (Fig. 2B). In order to determine whether the increase in biovolume required the presence of *P. aeruginosa* at the time of initial colonization, we added *P. aeruginosa* or a medium-only control to *C. albicans* 24-h-old biofilms. In these experiments, the *P. aeruginosa* cells were spiked into the chambers for 1 h, followed by a return to sterile ASMi medium. In control experiments, the same spiking procedure was performed but with sterile ASMi medium. While *C. albicans* biofilm accumulation followed its normal monoculture profile in the control condition, *C. albicans* biofilm development significantly increased over the subsequent 12 h after the introduction of *P. aeruginosa* (Fig. 2C). To determine whether any mechanical disturbance was sufficient to induce the increase in *C. albicans* biomass accumulation, we introduced 1-μm-diameter inert fluorescent beads to the chambers containing *C. albicans*, but we saw no change in biofilm architecture or biomass (Fig. S3).

The enhancement of *C. albicans* biofilm volume by the presence of *P. aeruginosa* was not likely due to an overall improvement in growth when both species are present. In comparison experiments in which both organisms were cultivated planktonically in shaking

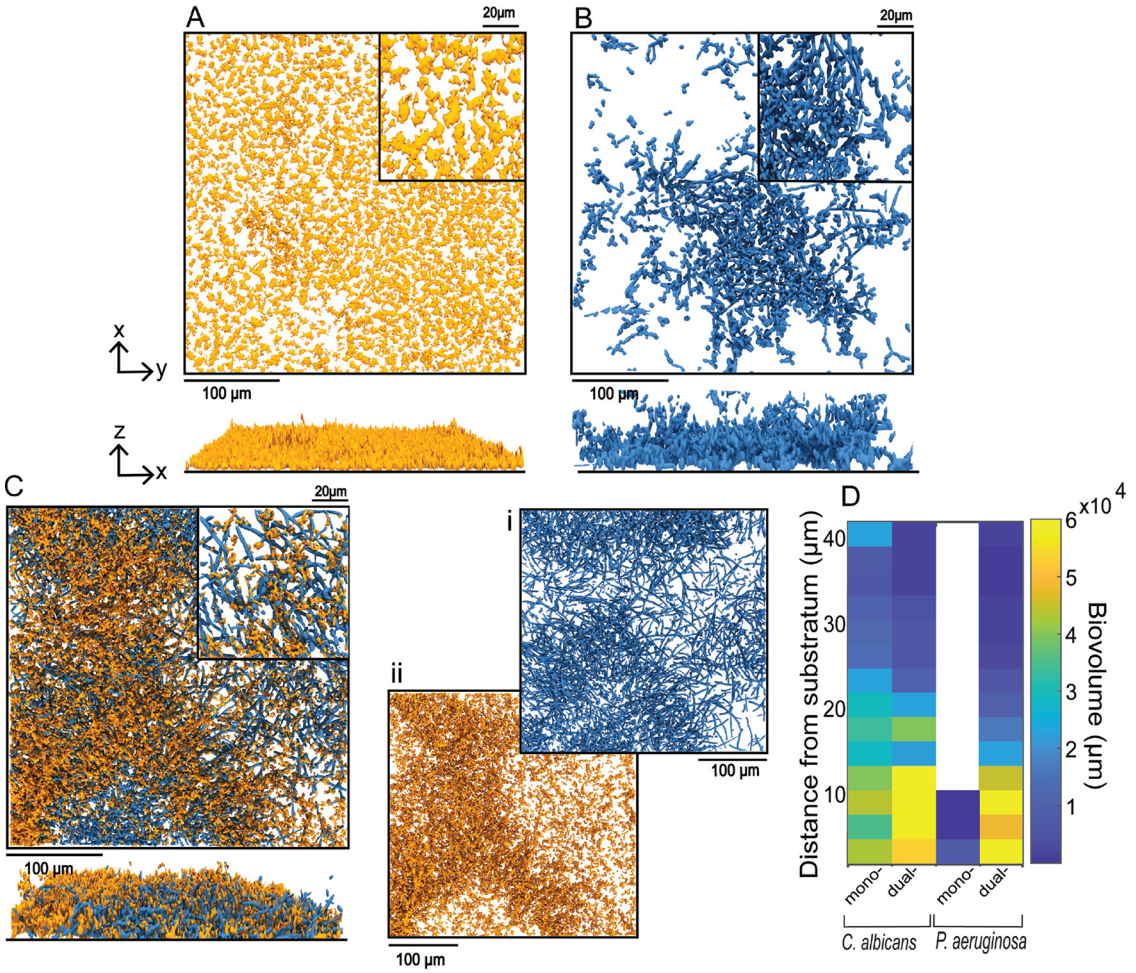

FIG 1 Representative images of mono- and dual-species biofilms of *P. aeruginosa* and *C. albicans*. Three-dimensional (3-D) renderings of 24-h-old monospecies biofilms of *P. aeruginosa* (A) and *C. albicans* (B). Bottom panels show side views of the same images as those above them. (C) *P. aeruginosa-C. albicans* dual-species biofilm at 24 h. Split channel of *C. albicans* biofilm (i) and *P. aeruginosa* biofilm (ii) from the *P. aeruginosa-C. albicans* dual-species biofilm. (D) Heat maps of *C. albicans* and *P. aeruginosa* biovolume as a function of height from the base substratum in mono- and dual-species biofilms from panels A to C.

liquid ASMi medium, the reverse pattern was seen for *C. albicans*: its population density was substantially lower in the presence of *P. aeruginosa* than in its absence (Fig. 2D), recapitulating previously established antagonistic *C. albicans-P. aeruginosa* interaction in liquid growth conditions (19, 28, 29). The population density of *P. aeruginosa* did not change in the presence of *C. albicans* in liquid culture (Fig. 2E). We infer from this outcome that the increase in accumulation of both species in microfluidic coculture is specific to the biofilm environment.

Because increased rate of biovolume increase can result from higher retention of cells in the chambers due to decreases in active dispersal or disruption by fluid flow, we quantified the cells in the effluent collected from the outlet of the microfluidic chambers (see Materials and Methods). Significantly fewer *C. albicans* cells were found in the effluent from dual-species biofilms (Fig. 2F). *P. aeruginosa* cell concentration in effluent stayed the same in absolute terms (Fig. 2F) but was lower upon normalization to the amount of biovolume in the biofilm chamber (Fig. S4).

Exploration of *P. aeruginosa* genes potentially involved in augmenting *C. albicans* biofilms in coculture. We repeated the mono- and coculture experiments above with mutants of *P. aeruginosa* that have been implicated in altered biofilm morphology or interspecies interaction in prior work. Analyses included mutants defective in the Pel exopolysaccharide production (Δ*pelA* [30, 31] and Δ*wspR* [32]), metabolic

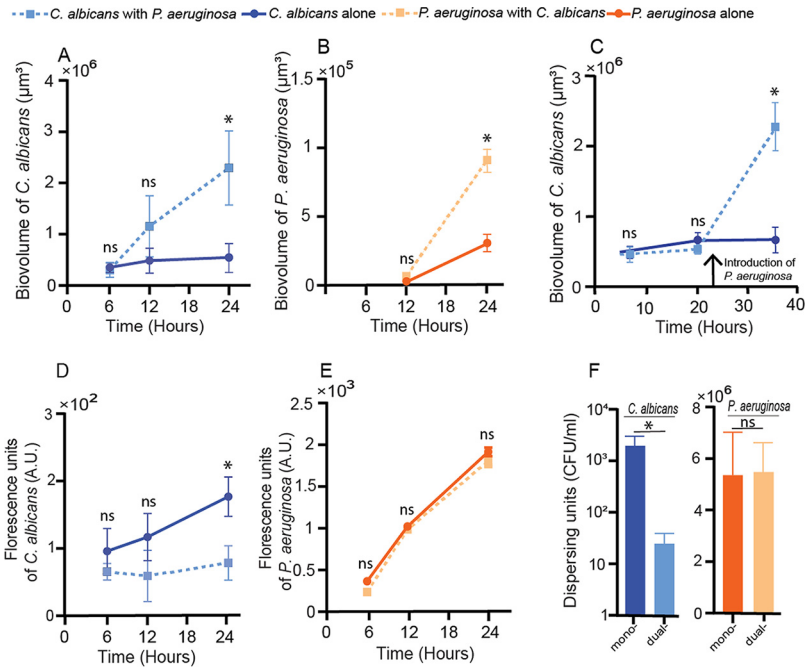

FIG 2 *P. aeruginosa* and *C. albicans* in mono- and dual-species culture. (A) Biovolume of *C. albicans* in mono- and dual-species biofilms ($n = 24$). (B) Biovolume of *P. aeruginosa* in mono- and dual-species biofilms ($n = 24$). (C) Biovolume of *C. albicans* biofilms initially grown in monoculture, with the addition of *P. aeruginosa* at the time point indicated by the vertical arrow. For the control, sterile medium was added in place of *P. aeruginosa* ($n = 18$). (D) Fluorescence counts of *C. albicans* in mono- and dual-species shaking liquid cultures ($n = 10$). (E) Fluorescence counts of *P. aeruginosa* (in arbitrary units [A.U.]) in mono- and dual-species shaking liquid cultures ($n = 10$). (F) Dispersing cells of *P. aeruginosa* and *C. albicans* in mono- and dual-species biofilms ($n = 11$). Error bars in panels A to E denote standard deviations; error bars in panel F denote standard errors. *, $P < 0.05$ by Wilcoxon signed-rank test with Bonferroni correction; ns, not significant.

regulators and products important for biofilm formation (Δ*anr* [33] and Δ*phz* [34]), extracellular adhesins (Δ*bapA* [35], Δ*pilY1* [36]), quorum sensing (Δ*lasR* [37]), and siderophore production (Δ*pvdApchE* [38]). *C. albicans* increased its accumulation by an order of magnitude or higher in biofilms with any of these mutants, maintaining the trend seen with wild-type *P. aeruginosa* PA14 (Fig. 3A and Fig. S5). In contrast, not all *P. aeruginosa* mutants were equal in their capacity for biofilm formation or for stimulation of biofilm biovolume in the presence of *C. albicans* (Fig. 3B). The Δ*pelA* and Δ*wspR* mutants were not defective in biofilm biovolume compared to the wild type, which is consistent with the low detection of Pel extracellular matrix carbohydrate (Fig. S6). Thus, the increased biovolume of *P. aeruginosa* was not due to increased *P. aeruginosa* matrix production. Previously characterized mutants defective in secreted phenazine toxins and pyochelin and pyoverdine siderophores also caused the stimulation of *C. albicans* biofilm accumulation. *P. aeruginosa* mutants with lower levels of monospecies biofilm (Δ*anr*, Δ*lasR*, Δ*bapA*, and Δ*pilY1*) were less stimulated by *C. albicans* at the 24-h time point. It is interesting to note that the amount of *P. aeruginosa* biofilm biomass present did not correlate with the degree of biomass increase in *C. albicans* (Fig. 3C); that is, any addition of *P. aeruginosa*, regardless of its native biofilm-producing capacity, was sufficient to produce a similar increase in accumulation of *C. albicans*.

***P. aeruginosa*-*C. albicans* interaction is robust to CF isolate variation.** After documenting that wild-type PA14 could induce an increase in biofilm biomass accumulation of *C. albicans*, we were curious to see whether this effect was consistent across recent CF clinical isolates of *P. aeruginosa* as well. To explore this question, we obtained *P. aeruginosa* clinical isolates from a patient who was infected with both *P. aeruginosa* and *C. albicans*, and we grew them in mono- or coculture with *C. albicans* in our microfluidic model under flow of ASMi. We found that *C. albicans* biofilm increased

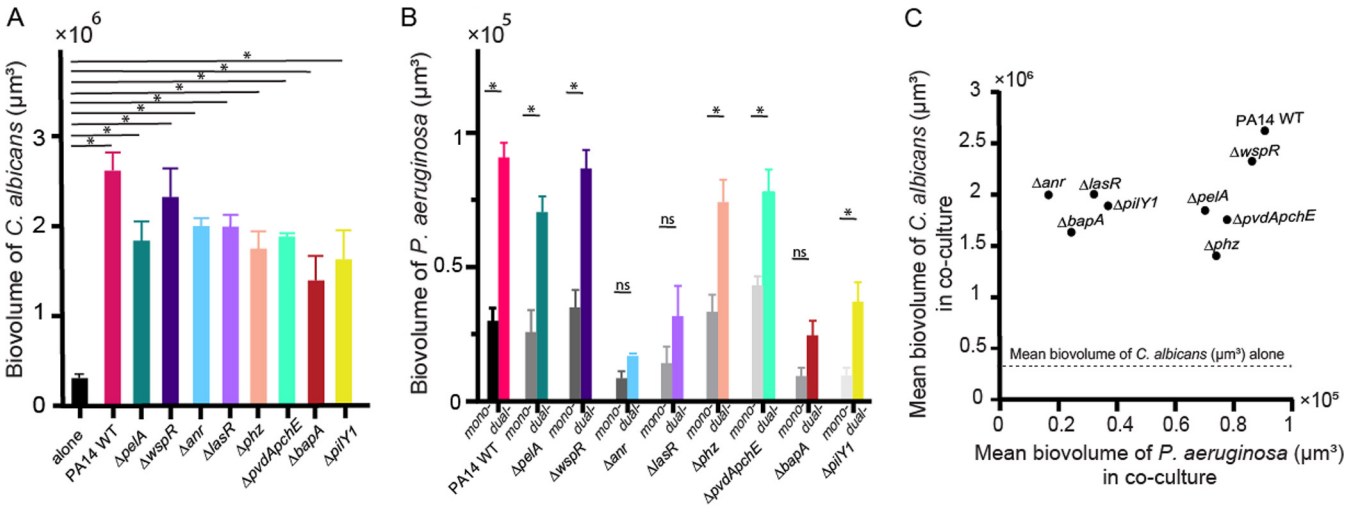

FIG 3 Deletion mutant assays and medium influent assays to explore the causes of mutual enhancement between *P. aeruginosa* and *C. albicans* in biofilms. (A) Biovolume of *C. albicans* grown in dual-species biofilms with *P. aeruginosa* deletion mutants at 24 h (see main text for mutant descriptions, $n = 9$ to 24). (B) Biovolumes of mono- and dual-species *P. aeruginosa* biofilms at 24 h ($n = 9$ to 24). All error bars indicated are standard errors. (C) The mean values of *C. albicans* biovolume are plotted against the corresponding mean value of wild-type (WT) *P. aeruginosa* PA14 and mutant biovolume from their respective dual-species biofilms. There is no significant correlation between the two (linear correlation analysis; $P = 0.391$; $r^2 = 0.107$). *, $P < 0.05$ by Wilcoxon signed-rank test with Bonferroni correction.

significantly in coculture with all clinical isolates, consistent with the results reported above for wild-type PA14 (Fig. 4A). Likewise, for all but one isolate, the biofilm growth of *P. aeruginosa* was greater in coculture with *C. albicans* than it was in monoculture (Fig. 4B).

Though all clinical *P. aeruginosa* isolates prompted an increase in *C. albicans* biofilm accumulation, there was some variance in the degree to which this was the case (Fig. 4A). This variation made us wonder whether the spatial association between *C. albicans* and different clinical isolates of *P. aeruginosa* might differ as well. To assess this possibility, we grew the different clinical isolates together with *C. albicans*, acquired high-resolution images of coculture biofilms, and quantified the spatial cooccurrence of the two species via their density correlation (39). When averaged across all image replicates, the spatial correlations between *C. albicans* and clinical isolates of *P. aeruginosa* generally were not different from that between *C. albicans* and wild-type PA14 (Fig. 4C). After visualizing the density correlation measurement at high spatial resolution, on the other hand (Fig. 4D), it was clear that for some clinical *P. aeruginosa* isolates, the spatial association with *C. albicans* was homogenous, while for others it was patchy. Previous work has suggested that heterogeneity within a strain population—here, with respect to spatial cooccurrence with *P. aeruginosa* and *C. albicans*—can impact survival in variable environmental conditions (40–42). The significance of this result for the infection ecology of these two species is not yet clear, but it is notable that among isolates of *P. aeruginosa* from the same patient, the architecture of joint biofilms with *C. albicans* can differ substantially at the micrometer scale (Fig. 4D) even when they appear to be the same or similar when averaged on a larger spatial scale (Fig. 4C).

DISCUSSION

Interest in multispecies biofilms including microbes from different domains of life has been intensifying in recent years, as it is increasingly appreciated that many microbial communities—both inside and outside host organisms—are polymicrobial (43). One of the most highly referenced examples of polymicrobial infections are those within the lungs of patients with CF, and two of the common members of these communities are the opportunistic pathogens *P. aeruginosa* and *C. albicans* (12). Here, we sought to compare the kinetics of biovolume accumulation in mono- and dual-species

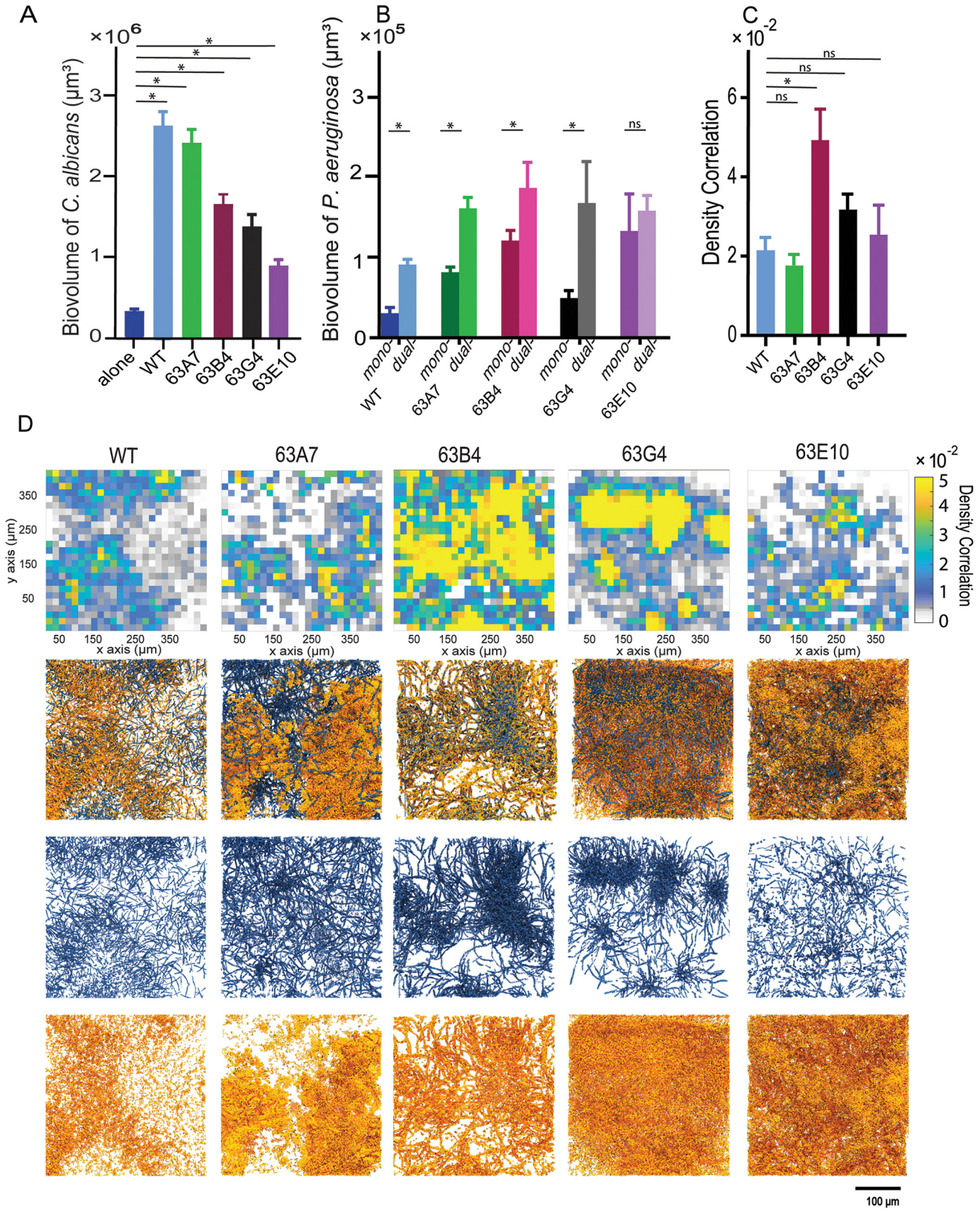

FIG 4 Biomass accumulation, density correlation analysis, and visualization of *C. albicans* in coculture with different CF clinical isolates of *P. aeruginosa*. (A) Biovolume of *C. albicans* grown as dual-species biofilms with *P. aeruginosa* clinical isolates along with wild-type (WT) PA14 for comparison at 24 h ($n = 18$). (B) Biovolumes of *P. aeruginosa* clinical isolates in monoculture and dual culture with *C. albicans* at 24 h ($n = 18$). (C) Global density correlation measurements of WT *P. aeruginosa* and clinical isolates and *C. albicans* biofilms ($n = 6$). *, $P < 0.05$. (D) Visualization of dual-species biofilms of *P. aeruginosa* and *C. albicans*. From top to bottom, spatially resolved density correlation, 3-D renderings of dual-species biofilms, *C. albicans* channel split, and *P. aeruginosa* channel split.

biofilms of these two organisms using a new model of biofilm growth under flow of optically clear artificial sputum medium. We demonstrated a marked increase of biofilm biomass accumulation as well as a decrease in cells in biofilm effluent in dual-species culture relative to monoculture. These results were robust to a variety of mutant and clinical strain backgrounds of *P. aeruginosa*, and they contrast with the findings of some previous studies of these two organisms in static liquid or agar colony culture (44, 45). We identify an important element driving the increase in biomass accumulation as fluid flow in the dual-species biofilm milieu, which is a key novelty of this experimental approach for the study of *P. aeruginosa-C. albicans* interactions.

Extensive prior work has shown that *P. aeruginosa* and *C. albicans* interact with each other through a complex web of secreted factors, including phenazines, siderophores, ethanol, and quorum-sensing autoinducers, which altogether alter environmental iron availability, pH, and oxygen tension. Under static culture conditions (i.e., liquid batch culture or agar colonies), the net result of these interactions is usually antagonism of *P. aeruginosa* against *C. albicans*. It is important to note as well that secreted factors from each species have different and sometimes opposite effects on each other's propensity to produce biofilms or to remain in a dispersive, planktonic state (28, 46). As noted above, when flow—known to impact microbial physiology and surface interaction—is introduced into the two-species system, we see increased filamentation of *C. albicans* and increased biofilm biomass accumulation by both species, accompanied by a decrease in cells exiting the chamber.

While at first glance this may give the impression of mutual benefit, it is also possible that the two species are simply competing for access to space and resources by upregulating adhesion factors (47–49). But why is *P. aeruginosa* no longer able to directly antagonize and kill *C. albicans*, as has been shown previously in static culture? We speculate that introduction of flow fundamentally changes the secreted solute environment created by the two organisms, perhaps with some secreted factors more strongly retained in the biofilm matrix than others, and that this change in solute environment relative to static culture shifts the ecological pattern of biomass accumulation to one in which both species are augmented. It is also possible that over time the dual-species biofilms become densely packed enough to block flow within some regions, allowing secreted products and variation in iron/oxygen availability to accumulate in a patchy manner that contributes to induction of biofilm production by both species. The precise spatial patterns of exoproduct accumulation in relation to cells and the highly complex matrix that *Candida* secretes is an important area for future work (50–52).

Our deletion mutant analysis included all the major classes of behavior in *P. aeruginosa* currently known to mediate solute-based interactions with *C. albicans*, but in all cases, the presence of *P. aeruginosa* caused qualitatively the same increase in *C. albicans* biofilm. This suggests that there may be other factors in addition to flow-mediated changes in solute environment contributing to our results. For example, the introduction of shear stress under flow is an entirely new environmental stimulus relative to static culture, and one which is known via extensive work to be crucial to microbial ecology and evolution (53–58). The flow regime can dramatically alter the morphology and resilience of bacterial biofilms down to their cellular resolution architecture (59, 60), with important implications for pathogenesis in the case of infections (61). Adaptation to the challenges of flow at submillimeter spatial scales has influenced the evolution of bacterial surface motility (2), optimal growth rate in porous media (62), surface colonization mechanisms (63–65), extracellular matrix secretion (66, 67), bacterial cell shape (64, 68–70), planktonic aggregate formation (71), and biofilm community assembly and function (62, 72–75), among many other examples.

The range of spatial structures of *P. aeruginosa* clinical isolates that we observed in dual-species biofilms with *C. albicans* suggests the possibility of between-strain variance in spatial occupation strategy within the CF lung. Since the clinical isolates come from a single CF patient, this variation in biofilm morphology could be the outcome of

selection in different spatial locations in the lung, which may have variable *C. albicans* abundance or exposure to antibiotics, toxins, mutagens, nutrient availability, or host immune attack (40, 41). Although the increase in biovolume of both species in dual *P. aeruginosa-C. albicans* biofilms varied to an extent, increase of *C. albicans* accumulation was consistent across *P. aeruginosa* isolates. This result prompts us to speculate that the chance encounter of *C. albicans* with *P. aeruginosa* in the CF environment could ultimately lead to changes in disease progression by altering the tendency of the fungus to locally accumulate.

In light of our results, it is important to note that the flow regime has documented effects on biofilm formation for both *P. aeruginosa* and *C. albicans*. The surface residence time of *P. aeruginosa*, for example, increases linearly as shear stress increases (76), and flow promotes upstream surface motility in addition to the formation of biofilm aggregates (77). *P. aeruginosa* has also recently been shown to be highly responsive to mechanical stress induced by flow, with downstream effects on biofilm formation that have yet to be fully clarified (36, 78). There has been less investigation of the effects of shear flow on *C. albicans* biofilms: existing work does not agree completely on whether shear stress increases total biomass of *C. albicans* biofilms but does agree that biofilms formed under shear are more highly compacted and physically robust relative to those grown in static conditions (79). Importantly, given that dual-species culture produced substantial biomass accumulation for both species relative to monoculture under the same flow conditions, flow-induced shear cannot on its own explain our results. Rather we infer that a combination of physical forces resulting from flow in addition to biological interaction between the two species must be responsible for the results obtained here. Dissecting the precise molecular mechanisms of these interspecies interactions is an important area for future study that may bear directly on the outcome of multispecies biofilm growth in the context of infection.

Beyond their prevalence in lung infections among patients with CF, *P. aeruginosa* and *C. albicans* individually are among the most common agents of nosocomial infection currently known (16). They are both frequently isolated from device-related infections, including implanted medical devices, prosthetic implants in wounds and joint replacements, and urinary catheters (16). Both species participate in multispecies infections, for example, with *Staphylococcus* spp. (80–82), with *Streptococcus* spp. (83, 84), and with each other (85). Reports of dual isolation of *P. aeruginosa* and *C. albicans* are increasingly reported in the clinical literature in sites such as ventilator tubing (86), and our results of biofilm dual-species culture in microfluidic devices suggest that dual *Pseudomonas-Candida* biofilms may be especially problematic in this setting because they tend to accumulate more biofilm biomass together than alone. Such rapidly accumulating biofilms can potentially clog catheter flow environments and seed systemic infections as cells disperse from the device-attached biofilm into the bloodstream.

Though recent studies have made tremendous strides in imaging microbiomes within *in situ* samples that have been fixed (87–90), dissecting live microbial community structure in space and time within native environments remains a challenging task and one of the important frontiers of modern microbiology. Here, we use an *in vitro* model with medium tuned to the CF sputum environment to assess live biofilm population dynamics for both members and find that this step toward environmental realism has a strong impact on the ecology of dual-species biofilms of *P. aeruginosa* and *C. albicans*. Many native factors are still missing, however: the mucosal environment is quite different in the native lung, for example, and recent work has suggested that mucus has a strong impact on *P. aeruginosa* physiology, including reducing its propensity toward virulence and biofilm formation (91, 92). Though not an exact match to the *in situ* infection environment, our system nevertheless suggests that modest changes to the environmental context in which multispecies interactions are studied can have a large impact on the observed outcome, namely, in this case, a shift toward far higher accumulation of biofilm on the part of *P. aeruginosa* and *C. albicans* when they are together versus when they are alone. On the basis of this observation, we speculate that

TABLE 1 Strains and plasmids used in this study

Species and strain	Relevant marker(s) or genotype(s)	Reference or source
E. coli		
S17-1	λ*pir*	Lorenzo and Timmis (100)
P. aeruginosa PA14		
CNP17	Wild type (WT)	Hogan lab
CNP26	WT with mKO-κ	This study
CNP12	Δ*pelA*	Friedman and Kolter (30)
CNP27	Δ*pelA* with mKO-κ	This study
CNP18	Δ*wspR*	Chen et al. (21)
CNP28	Δ*wspR* with mKO-κ	This study
CNP70	Δ*bapA*	Hogan lab
CNP77	Δ*bapA* with mKO-κ	This study
CNP65	Δ*pilY1*	Hogan lab
CNP67	Δ*pilY1* with mKO-κ	This study
CNP21	Δ*anr*	Hogan lab
CNP50	Δ*anr* with mKO-κ	This study
CNP69	Δ*pchEpvdA*	Hogan lab
CNP76	Δ*pchEpvdA* with mKO-κ	This study
CNP22	Δ*lasR*	Hogan lab
CNP56	Δ*lasR* with mKO-κ	This study
CNP41	Δ*phz*	Hogan lab
CNP54	Δ*phz* with mKO-κ	This study
CNP43	63LB4 clinical CF isolate	Hogan lab
CNP44	63LG4 clinical CF isolate	Hogan lab
CNP45	63RA7 clinical CF isolate	Hogan lab
CNP46	63RE10 clinical CF isolate	Hogan lab
CNP59	63LB4 clinical CF isolate with mKO-κ	This study
CNP57	63LG4 clinical CF isolate with mKO-κ	This study
CNP60	63RA7 clinical CF isolate with mKO-κ	This study
CNP58	63RE10 clinical CF isolate with mKO-κ	This study
C. albicans CAI4		
CNC1	WT with pACT-GFP	Hogan lab
CNC11	WT with pACT mKATE2	This study

pushing toward realism and high-resolution image analysis of biofilm communities will yield important and unexpected insights for many other microbial systems of interest.

MATERIALS AND METHODS

Strains and media. Table 1 includes a full list of strains and plasmids used in this study. Strains of *P. aeruginosa* are either derivatives of strain PA14 or clinical isolates. *C. albicans* strains are derivatives of strain CAI4. All strains were grown on LB (10 g tryptone, 5 g NaCl, 5 g yeast extract [all amounts per liter]) and artificial sputum medium for imaging (ASMi) (*P. aeruginosa*) or YPD (10 g yeast extract, 20 g peptone, and 20 g dextrose [all amounts per liter]) and ASMi (*C. albicans*). The medium recipes and concentrations of reagents used for ASMi are listed below at the end of Materials and Methods. All chemicals and reagents were purchased from Millipore Sigma unless otherwise stated.

Plasmid and strain construction. All restriction enzymes and ligase were purchased from New England Biolabs, and PCR reagents were purchased from Bio-Rad. The *P. aeruginosa* tandem codon-optimized version of *mKO-κ* was custom synthesized by Invitrogen. The construct contains two copies of *mKO-κ* in tandem, each with its own ribosome binding site, and with different codon composition to prevent excision by recombination. Fluorescent *P. aeruginosa* derivatives were constructed by amplification of the flanking regions upstream and downstream of the Tn*7 att* site and fusion of the custom fluorescent protein construct to a synthetic *tac* promoter for high expression from a single chromosomal locus. This fused construct was cloned into the pMQ30 plasmid used for allelic exchange in *P. aeruginosa* (93). This plasmid was then introduced into *Escherichia coli* S17-λ*pir* by electroporation and conjugated into *P. aeruginosa*, and recombinants were obtained using selection on gentamicin and sucrose counterselection for loss of the integrated plasmid backbone. For *C. albicans*, a single codon-optimized version of *mKate2* was custom synthesized by Invitrogen. The RP10 integrative plasmid, pACT-GFP (94), has been shown to have constant expression levels through *C. albicans* growth cycle. We replaced the green fluorescent protein (GFP) in pACT-GFP (94) with *mKate2*. For transformation into *C. albicans*, the *mKate2*-containing plasmid was linearized by BglII restriction digestion and concentrated using the Zymo Research DNA Clean & Concentrator-5 kit (catalog no. 11-303), and 1 μg was electroporated into electrocompetent *C. albicans* CAI4 prepared as previously described (95). Prototrophic recombinants were selected for on uracil drop-out medium.

Liquid growth curve and fluorescence measurements. *P. aeruginosa* strains were grown at 37°C shaking in LB overnight prior to growth curve experiments. The following morning, cultures were back-diluted to an optical density at 600 nm (OD_{600}) of 0.01 in ASMi in 10-ml glass tubes with 2 ml medium (for fluorescence growth curves) or 50-ml Falcon tubes with 30 ml of medium (optical density growth curves), rotating at 250 rpm on an incubated orbital shaker at 37°C. *C. albicans* strains were grown at 30°C shaking in YPD overnight prior to growth curve experiments. They were cultivated overnight at 30°C to maintain cells in yeast form prior to the start of growth curve or biofilm experiments (see below). The following morning, cultures were back-diluted to an OD_{600} of 0.01 in ASMi in 10-ml glass tubes with 2 ml medium (for fluorescence growth curves) or 50-ml Falcon tubes with 30 ml of medium (optical density growth curves), rotating at 250 rpm on an incubated orbital shaker at 37°C. Fluorescence measurements were made using a Synergy Neo2 every 6 h. A 543-nm excitation source was used to excite *mKO-κ*, and a 594-nm excitation source was used to excite *mKate2*. Optical density measurements were made every hour using a benchtop spectrophotometer (CWA Biowave CO8000 cell density meter).

Microfluidic device assembly. The microfluidic devices were made by bonding polydimethylsiloxane (PDMS) chamber molds to size #1.5 cover glass slips (60 mm × 36 mm [length *L* × width *W*], Thermo-Fisher, Waltham, MA) using standard soft lithography techniques (96). Each PDMS mold contained four chambers, each of which measured 3,000 μm × 500 μm × 75 μm (*L* × *W* × depth *D*). To establish flow in these chambers, medium was loaded into 1-ml BD plastic syringes with 25-gauge needles. These syringes were joined to #30 Cole-Parmer polytetrafluoroethylene (PTFE) tubing (inner diameter, 0.3 mm), which was connected to prebored holes in the microfluidic device. Tubing was also placed on the opposite end of the chamber to direct the effluent to a waste container. Syringes were mounted to syringe pumps (Pico Plus Elite, Harvard Apparatus), and flow was maintained at 0.1 μl per min for all experiments.

Biofilm growth, matrix staining, and CFU counts. Overnight cultures of *P. aeruginosa* were grown at 37°C with shaking in LB, and overnight cultures of *C. albicans* were grown at 30°C with shaking in YPD prior to the start of biofilm experiments. Cultures of both strains were normalized to an OD_{600} of 0.05 in ASMi medium. If dual-species biofilms were to be started, equal volumes of OD-equalized strains were mixed, inoculated into a microfluidic chamber (completely filling its inner volume), and then allowed to rest for 1 h at 37°C to permit cells to attach to the glass surface. The devices were then run at 0.1 μl per min at 37°C and imaged by confocal microscopy (see below) at time intervals that varied per experiment as noted in each figure. All experiments were repeated with at least five biological replicates with three or more technical replicates on different days. Total replicates for each experiment are noted in the figure legends for each data set in the text and supplemental material.

Wisteria floribunda lectin stain (Vector Labs) conjugated to fluorescein dye was used to visualize Pel polysaccharide produced by *P. aeruginosa* (31). The lectin was added to the medium in syringes for these experiments such that biofilms would be exposed to the lectin-dye conjugate for the entire period of biofilm growth (20 μl stock lectin solution per ml of medium, per the manufacturer's protocol recommendation from a stock solution of 2-mg/ml dye conjugate). Biofilms were inoculated as noted above for these experiments and grown for 24 h prior to imaging.

To compare growth rates of *P. aeruginosa* and *C. albicans* in turbid synthetic cystic fibrosis medium (SCFM) (25) and optically clear ASMi, both species were grown overnight, *P. aeruginosa* in LB at 37°C and *C. albicans* in YPD at 30°C in 10-ml glass tubes with 2 ml of medium. The following morning, the cultures were back-diluted to an OD_{600} of 0.01 in either SCFM or ASMi in 50-ml Falcon tubes with 30 ml of medium, rotating at 250 rpm in an orbital shaker at 37°C. One milliliter of culture was taken from the Falcon tube at different time points, and serial dilution was performed and plated on LB agar for *P. aeruginosa* and YPD agar for *C. albicans*. The number of CFU from each plate was recorded and used to calculate growth rates measured by CFU per milliliter per time.

To measure passive dispersal from biofilms as a result of exposure to fluid shear, biofilms of both species were grown as noted above in ASMi medium for 24 h, after which the outlet tubing of the microfluidic device was changed to ensure we were measuring dispersal only from the biofilms within the chambers themselves. The flow rate was increased to 500 μl per min, and outflow was collected. Serial dilutions were performed and plated on LB agar for *P. aeruginosa* and YPD containing 50 μg/ml chloramphenicol for *C. albicans*. The number of CFU from each plate was recorded and used to calculate the CFU/milliliter culture density emerging from the chambers. This experiment was repeated for 11 biological replicates with independent overnight cultures.

Microscopy and image analysis. Biofilms inside microfluidic chambers were imaged using a Zeiss LSM 880 confocal microscope with a 40×/1.2 numerical aperture (NA) or 10×/0.4 NA water objective. A 543-nm laser line was used to excite mKO-κ, and a 594-nm laser line was used to excite mKate2. A 458-nm laser line was used to excite *Wisteria floribunda* lectin stain in the case of Pel quantification experiments. All quantitative analysis of microscopy data was performed using BiofilmQ (39). Three-dimensional (3-D) renderings of biofilms in Fig. 1 and 4 were made using Paraview.

Statistics. All statistical analyses were performed in GraphPad Prism. All reported pairwise comparisons were performed using Wilcoxon signed-rank tests, and multiple comparisons were performed by Wilcoxon signed-rank tests with Bonferroni correction. All error bars indicated standard errors unless otherwise noted.

Artificial sputum media for imaging (ASMi). The stocks for the base were Na_2HPO_4 (0.2 M, 0.69 g/25 ml), NaH_2PO_4 (0.2 M, 0.71 g/25 ml), KNO_3 (1 M, 2.53 g/25 ml), K_2SO_4 (0.25 M, 1.09 g/25 ml). Additional stocks were glucose (20% [wt/vol]) autoclave, L-lactic acid (1 M) (adjust pH to 7 with NaOH), $CaCl_2 \cdot 2H_2O$ (1 M, 3.68 g/25 ml), $MgCl_2 \cdot 6H_2O$ (1 M, 5.08 g/25 ml), $FeSO_4 \cdot 7H_2O$ (1 mg/1 ml) syringe, *N*-acetylglucosamine (0.25 M, 1.383 g/25 ml), tryptophan (0.1 M, 1.021 g/50 ml). Reagents were DNA (herring sperm

DNA), fucose, GalNAc, galactose, choline chloride, sodium octanoate, yeast synthetic dropout excluding Trp, NaCl, morpholinepropanesulfonic acid (MOPS), KCl, NH_4Cl, and NaOH. Preparation of ASMi (500 ml) (2× in 250 ml) was as follows: 1) add 400 ml distilled H_2O (diH_2O) and stir bar to a clean beaker; 2) while stirring add 3.250 ml Na_2HPO_4 stock, 3.126 ml NaH_2PO_4 stock, 174 μl KNO_3 stock, 542 μl K_2SO_4 stock, 2 g yeast synthetic dropout – Trp, 1.516 g NaCl, 1.046 g morpholinepropanesulfonic acid (MOPS), 558 mg KCl, 62 mg NH_4Cl, 4.65 ml L-lactic acid stock, 1.365 ml glucose stock, 875 μl $CaCl_2 \cdot 2H_2O$ stock, 600 μl *N*-acetylglucosamine, 500 μl $FeSO_4 \cdot 7H_2O$, 330 μl tryptophan stock, 303 μl $MgCl_2 \cdot 6H_2O$, 300 mg DNA, 0.007 g choline chloride, 0.022 g sodium octanoate (replacement 1,2-dipalmitoyl-*sn*-glycero-3-phosphocholine [DPPC]), 400 mg fucose, 125 mg GalNAc, 90 mg galactose, (replacement for mucin; these are mucin sugars); 3) adjust pH to 6.8 with HCl or NaOH and add distilled H_2O to 500 ml; 4) filter sterilize.

Considerations and references. Considerations follow. (i) It lacks sphingolipids and surfactant proteins, which are moderately abundant. (ii) Mucin sugars are used instead of mucin (97). (iii) Reports of some concentrations vary from source to source. References follow: DPPC (98) (octanoate and choline are used instead at the same concentrations; 2:1 octanoate-choline, since DPPC has two lipid chains per choline. DPPC molarity for choline and 2× that for octanoate), DNA (98), and mucin (98).

SUPPLEMENTAL MATERIAL

Supplemental material is available online only.

FIG S1, TIF file, 2.6 MB.

FIG S2, TIF file, 0.4 MB.

FIG S3, TIF file, 1.2 MB.

FIG S4, TIF file, 0.1 MB.

FIG S5, TIF file, 0.3 MB.

FIG S6, TIF file, 0.1 MB.

ACKNOWLEDGMENTS

We thank members of the Nadell and Hogan labs for their comments throughout the project, as well as the Dartmouth Cystic Fibrosis Research Center. Comments from David Andes were also invaluable for composing the paper. C.D.N. is supported by the Cystic Fibrosis Foundation grant STANTO15RO, NSF grant MCB 1817342, NSF grant IOS 2017879, a Burke Award from Dartmouth, NIH grant 2R01AI081838 to principal investigator (PI) Robert Cramer, NIH grant P20-GM113132 to the Dartmouth BioMT COBRE, and grant RGY0077/2020 from the Human Frontier Science Foundation with co-PI Alexandre Persat. Additional support was provided by the Cystic Fibrosis Foundation via STANTO19RO, HOGAN19GO and NIDDK P30-DK117469 (D.A.H.), and from the NIH to D.L.M. via grant T32AI007519.

We have no conflicts of interest to declare.

C.D.N. and D.A.H. conceived and supervised the project. S.K., D.L.M., D.A.H., and C.D.N. designed experiments. S.K. performed experiments and image analysis. S.K. and C.D.N. finalized figures. D.L.M. and D.A.H. contributed critical reagents. S.K., D.L.M., D.A.H., and C.D.N. wrote the paper.

REFERENCES

1. Nadell CD, Drescher K, Foster KR. 2016. Spatial structure, cooperation and competition in biofilms. Nat Rev Microbiol 14:589–600. https://doi.org/10.1038/nrmicro.2016.84.
2. Dufrêne YF, Persat A. 2020. Mechanomicrobiology: how bacteria sense and respond to forces. Nat Rev Microbiol 18:227–240. https://doi.org/10.1038/s41579-019-0314-2.
3. Flemming H-C, Wingender J, Szewzyk U, Steinberg P, Rice SA, Kjelleberg S. 2016. Biofilms: an emergent form of bacterial life. Nat Rev Microbiol 14:563–575. https://doi.org/10.1038/nrmicro.2016.94.
4. Elias S, Banin E. 2012. Multi-species biofilms: living with friendly neighbors. FEMS Microbiol Rev 36:990–1004. https://doi.org/10.1111/j.1574-6976.2012.00325.x.
5. Bispo P, Haas W, Gilmore M. 2015. Biofilms in infections of the eye. Pathogens 4:111–136. https://doi.org/10.3390/pathogens4010111.
6. Bowen WH, Burne RA, Wu H, Koo H. 2018. Oral biofilms: pathogens, matrix, and polymicrobial interactions in microenvironments. Trends Microbiol 26:229–242. https://doi.org/10.1016/j.tim.2017.09.008.
7. Silverstein A, Donatucci CF. 2003. Bacterial biofilms and implantable prosthetic devices. Int J Impot Res 15:S150–S154. https://doi.org/10.1038/sj.ijir.3901093.
8. Zhao G, Usui ML, Lippman SI, James GA, Stewart PS, Fleckman P, Olerud JE. 2013. Biofilms and inflammation in chronic wounds. Adv Wound Care 2:389–399. https://doi.org/10.1089/wound.2012.0381.
9. Filkins LM, O'Toole GA. 2015. Cystic fibrosis lung infections: polymicrobial, complex, and hard to treat. PLoS Pathog 11:e1005258. https://doi.org/10.1371/journal.ppat.1005258.
10. Ciofu O, Tolker-Nielsen T, Jensen PØ, Wang H, Høiby N. 2015. Antimicrobial resistance, respiratory tract infections and role of biofilms in lung infections in cystic fibrosis patients. Adv Drug Deliv Rev 85:7–23. https://doi.org/10.1016/j.addr.2014.11.017.
11. Stacy A, McNally L, Darch SE, Brown SP, Whiteley M. 2016. The biogeography of polymicrobial infection. Nat Rev Microbiol 14:93–105. https://doi.org/10.1038/nrmicro.2015.8.
12. Grahl N, Dolben EL, Filkins LM, Crocker AW, Willger SD, Morrison HG, Sogin ML, Ashare A, Gifford AH, Jacobs NJ, Schwartzman JD, Hogan DA. 2018. Profiling of bacterial and fungal microbial communities in cystic fibrosis sputum using RNA. mSphere 3:e00292-18. https://doi.org/10.1128/mSphere.00292-18.
13. Cutting GR. 2015. Cystic fibrosis genetics: from molecular understanding to clinical application. Nat Rev Genet 16:45–56. https://doi.org/10.1038/nrg3849.

14. Peters BM, Jabra-Rizk MA, O'May GA, Costerton JW, Shirtliff ME. 2012. Polymicrobial interactions: impact on pathogenesis and human disease. Clin Microbiol Rev 25:193–213. https://doi.org/10.1128/CMR.00013-11.
15. Fourie R, Pohl CH. 2019. Beyond antagonism: the interaction between Candida species and Pseudomonas aeruginosa. J Fungi 5:34. https://doi.org/10.3390/jof5020034.
16. Pierce GE. 2005. Pseudomonas aeruginosa, Candida albicans, and device-related nosocomial infections: implications, trends, and potential approaches for control. J Ind Microbiol Biotechnol 32:309–318. https://doi.org/10.1007/s10295-005-0225-2.
17. Nobile CJ, Johnson AD. 2015. *Candida albicans* biofilms and human disease. Annu Rev Microbiol 69:71–92. https://doi.org/10.1146/annurev-micro-091014-104330.
18. Moradali MF, Ghods S, Rehm BHA. 2017. Pseudomonas aeruginosa lifestyle: a paradigm for adaptation, survival, and persistence. Front Cell Infect Microbiol 7:39. https://doi.org/10.3389/fcimb.2017.00039.
19. Hogan DA, Kolter R. 2002. Interactions: an ecological role for virulence factors. Science 296:2229−2232. https://doi.org/10.1126/science.1070784.
20. Christiaen SEA, Matthijs N, Zhang X-H, Nelis HJ, Bossier P, Coenye T. 2014. Bacteria that inhibit quorum sensing decrease biofilm formation and virulence in *Pseudomonas aeruginosa* PAO1. Pathog Dis 70:271–279. https://doi.org/10.1111/2049-632X.12124.
21. Chen AI, Dolben EF, Okegbe C, Harty CE, Golub Y, Thao S, Ha DG, Willger SD, O'Toole GA, Harwood CS, Dietrich LE, Hogan DA. 2014. Candida albicans ethanol stimulates Pseudomonas aeruginosa WspR-controlled biofilm formation as part of a cyclic relationship involving phenazines. PLoS Pathog 10:e1004480. https://doi.org/10.1371/journal.ppat.1004480.
22. Lewis KA, Baker AE, Chen AI, Harty CE, Kuchma SL, O'Toole GA, Hogan DA. 2019. Ethanol decreases *Pseudomonas aeruginosa* flagellar motility through the regulation of flagellar stators. J Bacteriol 201:e00285-19. https://doi.org/10.1128/JB.00285-19.
23. Grahl N, Demers EG, Lindsay AK, Harty CE, Willger SD, Piispanen AE, Hogan DA. 2015. Mitochondrial activity and Cyr1 are key regulators of Ras1 activation of C. albicans virulence pathways. PLoS Pathog 11: e1005133. https://doi.org/10.1371/journal.ppat.1005133.
24. Bergeron AC, Seman BG, Hammond JH, Archambault LS, Hogan DA, Wheeler RT. 2017. Candida albicans and Pseudomonas aeruginosa interact to enhance virulence of mucosal infection in transparent zebrafish. Infect Immun 85:e00475-17. https://doi.org/10.1128/IAI.00475-17.
25. Turner KH, Wessel AK, Palmer GC, Murray JL, Whiteley M. 2015. Essential genome of *Pseudomonas aeruginosa* in cystic fibrosis sputum. Proc Natl Acad Sci U S A 112:4110–4115. https://doi.org/10.1073/pnas.1419677112.
26. Darch SE, Simoska O, Fitzpatrick M, Barraza JP, Stevenson KJ, Bonnecaze RT, Shear JB, Whiteley M. 2018. Spatial determinants of quorum signaling in a *Pseudomonas aeruginosa* infection model. Proc Natl Acad Sci U S A 115:4779–4784. https://doi.org/10.1073/pnas.1719317115.
27. Flynn JM, Niccum D, Dunitz JM, Hunter RC. 2016. Evidence and role for bacterial mucin degradation in cystic fibrosis airway disease. PLoS Pathog 12:e1005846. https://doi.org/10.1371/journal.ppat.1005846.
28. Hogan DA, Vik Å, Kolter R. 2004. A Pseudomonas aeruginosa quorum-sensing molecule influences Candida albicans morphology: Pseudomonas inhibition of C. albicans filamentation. Mol Microbiol 54:1212–1223. https://doi.org/10.1111/j.1365-2958.2004.04349.x.
29. Morales DK, Hogan DA. 2010. Candida albicans interactions with bacteria in the context of human health and disease. PLoS Pathog 6:e1000886. https://doi.org/10.1371/journal.ppat.1000886.
30. Friedman L, Kolter R. 2004. Genes involved in matrix formation in Pseudomonas aeruginosa PA14 biofilms. Mol Microbiol 51:675–690. https://doi.org/10.1046/j.1365-2958.2003.03877.x.
31. Jennings LK, Storek KM, Ledvina HE, Coulon C, Marmont LS, Sadovskaya I, Secor PR, Tseng BS, Scian M, Filloux A, Wozniak DJ, Howell PL, Parsek MR. 2015. Pel is a cationic exopolysaccharide that cross-links extracellular DNA in the *Pseudomonas aeruginosa* biofilm matrix. Proc Natl Acad Sci U S A 112:11353–11358. https://doi.org/10.1073/pnas.1503058112.
32. Hickman JW, Tifrea DF, Harwood CS. 2005. A chemosensory system that regulates biofilm formation through modulation of cyclic diguanylate levels. Proc Natl Acad Sci U S A 102:14422–14427. https://doi.org/10.1073/pnas.0507170102.
33. Jackson AA, Gross MJ, Daniels EF, Hampton TH, Hammond JH, Vallet-Gely I, Dove SL, Stanton BA, Hogan DA. 2013. Anr and its activation by PlcH activity in Pseudomonas aeruginosa host colonization and virulence. J Bacteriol 195:3093–3104. https://doi.org/10.1128/JB.02169-12.
34. Dietrich LEP, Okegbe C, Price-Whelan A, Sakhtah H, Hunter RC, Newman DK. 2013. Bacterial community morphogenesis is intimately linked to the intracellular redox state. J Bacteriol 195:1371–1380. https://doi.org/10.1128/JB.02273-12.
35. de Bentzmann S, Giraud C, Bernard CS, Calderon V, Ewald F, Plésiat P, Nguyen C, Grunwald D, Attree I, Jeannot K, Fauvarque MO, Bordi C. 2012. Unique biofilm signature, drug susceptibility and decreased virulence in Drosophila through the Pseudomonas aeruginosa two-component system PprAB. PLoS Pathog 8:e1003052. https://doi.org/10.1371/journal.ppat.1003052.
36. Rodesney CA, Roman B, Dhamani N, Cooley BJ, Katira P, Touhami A, Gordon VD. 2017. Mechanosensing of shear by *Pseudomonas aeruginosa* leads to increased levels of the cyclic-di-GMP signal initiating biofilm development. Proc Natl Acad Sci U S A 114:5906–5911. https://doi.org/10.1073/pnas.1703255114.
37. O'Loughlin CT, Miller LC, Siryaporn A, Drescher K, Semmelhack MF, Bassler BL. 2013. A quorum-sensing inhibitor blocks Pseudomonas aeruginosa virulence and biofilm formation. Proc Natl Acad Sci U S A 110:17981–17986. https://doi.org/10.1073/pnas.1316981110.
38. Harrison F, Buckling A. 2009. Siderophore production and biofilm formation as linked social traits. ISME J 3:632–634. https://doi.org/10.1038/ismej.2009.9.
39. Hartmann R, Jeckel H, Jelli E, Singh PK, Vaidya S, Bayer M, Vidakovic L, Díaz-Pascual F, Fong JCN, Dragoš A, Besharova O, Nadell CD, Sourjik V, Kovács AT, Yildiz FH, Drescher K. 2019. BiofilmQ, a software tool for quantitative image analysis of microbial biofilm communities. https://doi.org/10.1101/735423.
40. Magdanova LA, Golyasnaya NV. 2013. Heterogeneity as an adaptive trait of microbial populations. Microbiology 82:1–10. https://doi.org/10.1134/S0026261713010074.
41. Grote J, Krysciak D, Streit WR. 2015. Phenotypic heterogeneity, a phenomenon that may explain why quorum sensing does not always result in truly homogenous cell behavior. Appl Environ Microbiol 81:5280–5289. https://doi.org/10.1128/AEM.00900-15.
42. Hogan DA, Gladfelter AS. 2015. Editorial overview: host-microbe interactions: fungi: heterogeneity in fungal cells, populations, and communities. Curr Opin Microbiol 26:vii–vix. https://doi.org/10.1016/j.mib.2015.07.003.
43. Yang L, Liu Y, Wu H, Hóiby N, Molin S, Song ZJ. 2011. Current understanding of multi-species biofilms. Int J Oral Sci 3:74–81. https://doi.org/10.4248/IJOS11027.
44. Peleg AY, Hogan DA, Mylonakis E. 2010. Medically important bacterial–fungal interactions. Nat Rev Microbiol 8:340–349. https://doi.org/10.1038/nrmicro2313.
45. Trejo-Hernández A, Andrade-Domínguez A, Hernández M, Encarnación S. 2014. Interspecies competition triggers virulence and mutability in Candida albicans–Pseudomonas aeruginosa mixed biofilms. ISME J 8:1974–1988. https://doi.org/10.1038/ismej.2014.53.
46. Morales DK, Grahl N, Okegbe C, Dietrich LE, Jacobs NJ, Hogan DA. 2013. Control of Candida albicans metabolism and biofilm formation by Pseudomonas aeruginosa phenazines. mBio 4:e00526-12. https://doi.org/10.1128/mBio.00526-12.
47. Nadell CD, Xavier JB, Foster KR. 2009. The sociobiology of biofilms. FEMS Microbiol Rev 33:206–224. https://doi.org/10.1111/j.1574-6976.2008.00150.x.
48. Oliveira NM, Martinez-Garcia E, Xavier J, Durham WM, Kolter R, Kim W, Foster KR. 2015. Biofilm formation as a response to ecological competition. PLoS Biol 13:e1002191. https://doi.org/10.1371/journal.pbio.1002191.
49. Schluter J, Nadell CD, Bassler BL, Foster KR. 2015. Adhesion as a weapon in microbial competition. ISME J 9:139–149. https://doi.org/10.1038/ismej.2014.174.
50. Al-Fattani MA. 2006. Biofilm matrix of Candida albicans and Candida tropicalis: chemical composition and role in drug resistance. J Med Microbiol 55:999–1008. https://doi.org/10.1099/jmm.0.46569-0.
51. Zarnowski R, Sanchez H, Covelli AS, Dominguez E, Jaromin A, Bernhardt J, Mitchell KF, Heiss C, Azadi P, Mitchell A, Andes DR. 2018. Candida albicans biofilm–induced vesicles confer drug resistance through matrix biogenesis. PLoS Biol 16:e2006872. https://doi.org/10.1371/journal.pbio.2006872.
52. Mitchell KF, Zarnowski R, Sanchez H, Edward JA, Reinicke EL, Nett JE, Mitchell AP, Andes DR. 2015. Community participation in biofilm matrix assembly and function. Proc Natl Acad Sci U S A 112:4092–4097. https://doi.org/10.1073/pnas.1421437112.
53. Rusconi R, Stocker R. 2015. Microbes in flow. Curr Opin Microbiol 25:1–8. https://doi.org/10.1016/j.mib.2015.03.003.

54. Wheeler JD, Secchi E, Rusconi R, Stocker R. 2019. Not just going with the flow: the effects of fluid flow on bacteria and plankton. Annu Rev Cell Dev Biol 35:213–237. https://doi.org/10.1146/annurev-cellbio-100818-125119.
55. Yawata Y, Nguyen J, Stocker R, Rusconi R. 2016. Microfluidic studies of biofilm formation in dynamic environments. J Bacteriol 198:2589–2595. https://doi.org/10.1128/JB.00118-16.
56. Rusconi R, Garren M, Stocker R. 2014. Microfluidics expanding the frontiers of microbial ecology. Annu Rev Biophys 43:65–91. https://doi.org/10.1146/annurev-biophys-051013-022916.
57. Persat A, Nadell CD, Kim MK, Ingremeau F, Siryaporn A, Drescher K, Wingreen NS, Bassler BL, Gitai Z, Stone HA. 2015. The mechanical world of bacteria. Cell 161:988–997. https://doi.org/10.1016/j.cell.2015.05.005.
58. Nadell CD, Bucci V, Drescher K, Levin SA, Bassler BL, Xavier JB. 2013. Cutting through the complexity of cell collectives. Proc R Soc B 280:20122770. https://doi.org/10.1098/rspb.2012.2770.
59. Hartmann R, Singh PK, Pearce P, Mok R, Song B, Díaz-Pascual F, Dunkel J, Drescher K. 2019. Emergence of three-dimensional order and structure in growing biofilms. Nat Phys 15:251–256. https://doi.org/10.1038/s41567-018-0356-9.
60. Liu Y, Tay J-H. 2002. The essential role of hydrodynamic shear force in the formation of biofilm and granular sludge. Water Res 36:1653–1665. https://doi.org/10.1016/S0043-1354(01)00379-7.
61. Stewart PS. 2014. Biophysics of biofilm infection. Pathog Dis 70:212–218. https://doi.org/10.1111/2049-632X.12118.
62. Ebrahimi A, Schwartzman J, Cordero OX. 2019. Cooperation and spatial self-organization determine rate and efficiency of particulate organic matter degradation in marine bacteria. Proc Natl Acad Sci U S A 116:23309–23316. https://doi.org/10.1073/pnas.1908512116.
63. Kannan A, Yang Z, Kim MK, Stone HA, Siryaporn A. 2018. Dynamic switching enables efficient bacterial colonization in flow. Proc Natl Acad Sci U S A 115:5438–5443. https://doi.org/10.1073/pnas.1718813115.
64. Persat A, Stone HA, Gitai Z. 2014. The curved shape of Caulobacter crescentus enhances surface colonization in flow. Nat Commun 5:3824. https://doi.org/10.1038/ncomms4824.
65. Secchi E, Vitale A, Miño GL, Kantsler V, Eberl L, Rusconi R, Stocker R. 2020. The effect of flow on swimming bacteria controls the initial colonization of curved surfaces. Nat Commun 11:2851. https://doi.org/10.1038/s41467-020-16620-y.
66. Nadell CD, Ricaurte D, Yan J, Drescher K, Bassler BL. 2017. Flow environment and matrix structure interact to determine spatial competition in Pseudomonas aeruginosa biofilms. Elife 6:e21855. https://doi.org/10.7554/eLife.21855.
67. Martínez-García R, Nadell CD, Hartmann R, Drescher K, Bonachela JA. 2018. Cell adhesion and fluid flow jointly initiate genotype spatial distribution in biofilms. PLoS Comput Biol 14:e1006094. https://doi.org/10.1371/journal.pcbi.1006094.
68. Wucher BR, Bartlett TM, Hoyos M, Papenfort K, Persat A, Nadell CD. 2019. Vibrio cholerae filamentation promotes chitin surface attachment at the expense of competition in biofilms. Proc Natl Acad Sci U S A 116:14216–14221. https://doi.org/10.1073/pnas.1819016116.
69. Young KD. 2006. The selective value of bacterial shape. Microbiol Mol Biol Rev 70:660–703. https://doi.org/10.1128/MMBR.00001-06.
70. Yang DC, Blair KM, Salama NR. 2016. Staying in shape: the impact of cell shape on bacterial survival in diverse environments. Microbiol Mol Biol Rev 80:187–203. https://doi.org/10.1128/MMBR.00031-15.
71. Rusconi R, Guasto JS, Stocker R. 2014. Bacterial transport suppressed by fluid shear. Nature Phys 10:212–217. https://doi.org/10.1038/nphys2883.
72. Besemer K, Singer G, Hödl I, Battin TJ. 2009. Bacterial community composition of stream biofilms in spatially variable-flow environments. Appl Environ Microbiol 75:7189–7195. https://doi.org/10.1128/AEM.01284-09.
73. Besemer K, Singer G, Limberger R, Chlup AK, Hochedlinger G, Hödl I, Baranyi C, Battin TJ. 2007. Biophysical controls on community succession in stream biofilms. Appl Environ Microbiol 73:4966–4974. https://doi.org/10.1128/AEM.00588-07.
74. Rossy T, Nadell CD, Persat A. 2019. Cellular advective-diffusion drives the emergence of bacterial surface colonization patterns and heterogeneity. Nat Commun 10:2471. https://doi.org/10.1038/s41467-019-10469-6.
75. Besemer K, Peter H, Logue JB, Langenheder S, Lindström ES, Tranvik LJ, Battin TJ. 2012. Unraveling assembly of stream biofilm communities. ISME J 6:1459–1468. https://doi.org/10.1038/ismej.2011.205.
76. Lecuyer S, Rusconi R, Shen Y, Forsyth A, Vlamakis H, Kolter R, Stone HA. 2011. Shear stress increases the residence time of adhesion of Pseudomonas aeruginosa. Biophys J 100:341−350. https://doi.org/10.1016/j.bpj.2010.11.078.
77. Siryaporn A, Kim MK, Shen Y, Stone HA, Gitai Z. 2015. Colonization, competition, and dispersal of pathogens in fluid flow networks. Curr Biol 25:1201–1207. https://doi.org/10.1016/j.cub.2015.02.074.
78. Dingemans J, Monsieurs P, Yu S-H, Crabbé A, Förstner KU, Malfroot A, Cornelis P, Van Houdt R. 2016. Effect of shear stress on *Pseudomonas aeruginosa* isolated from the cystic fibrosis lung. mBio 7:e00813-16. https://doi.org/10.1128/mBio.00813-16.
79. Mukherjee PK, Chand DV, Chandra J, Anderson JM, Ghannoum MA. 2009. Shear stress modulates the thickness and architecture of Candida albicans biofilms in a phase-dependent manner. Mycoses 52:440–446. https://doi.org/10.1111/j.1439-0507.2008.01632.x.
80. Alves PM, Al-Badi E, Withycombe C, Jones PM, Purdy KJ, Maddocks SE. 2018. Interaction between Staphylococcus aureus and Pseudomonas aeruginosa is beneficial for colonisation and pathogenicity in a mixed biofilm. Pathog Dis https://doi.org/10.1093/femspd/fty003.
81. Carolus H, Van Dyck K, Van Dijck P. 2019. Candida albicans and Staphylococcus species: a threatening twosome. Front Microbiol 10:2162. https://doi.org/10.3389/fmicb.2019.02162.
82. Orazi G, Ruoff KL, O'Toole GA. 2019. *Pseudomonas aeruginosa* increases the sensitivity of biofilm-grown *Staphylococcus aureus* to membrane-targeting antiseptics and antibiotics. mBio 10:e01501-19. https://doi.org/10.1128/mBio.01501-19.
83. Shing SR, Ramos AR, Patras KA, Riestra AM, McCabe S, Nizet V, Coady A. 2020. The fungal pathogen Candida albicans promotes bladder colonization of group B Streptococcus. Front Cell Infect Microbiol 9:437. https://doi.org/10.3389/fcimb.2019.00437.
84. Scoffield JA, Duan D, Zhu F, Wu H. 2017. A commensal streptococcus hijacks a Pseudomonas aeruginosa exopolysaccharide to promote biofilm formation. PLoS Pathog 13:e1006300. https://doi.org/10.1371/journal.ppat.1006300.
85. Gibson J, Sood A, Hogan DA. 2009. Pseudomonas aeruginosa-Candida albicans interactions: localization and fungal toxicity of a phenazine derivative. Appl Environ Microbiol 75:504–513. https://doi.org/10.1128/AEM.01037-08.
86. Azoulay E, Timsit JF, Tafflet M, de Lassence A, Darmon M, Zahar JR, Adrie C, Garrouste-Orgeas M, Cohen Y, Mourvillier B, Schlemmer B, Outcomerea Study Group. 2006. Candida colonization of the respiratory tract and subsequent Pseudomonas ventilator-associated pneumonia. Chest 129:110–117. https://doi.org/10.1378/chest.129.1.110.
87. Earle KA, Billings G, Sigal M, Lichtman JS, Hansson GC, Elias JE, Amieva MR, Huang KC, Sonnenburg JL. 2015. Quantitative imaging of gut microbiota spatial organization. Cell Host Microbe 18:478–488. https://doi.org/10.1016/j.chom.2015.09.002.
88. Welch JLM, Rossetti BJ, Rieken CW, Dewhirst FE, Borisy GG. 2016. Biogeography of a human oral microbiome at the micron scale. Proc Natl Acad Sci U S A 113:E791–E800. https://doi.org/10.1073/pnas.1522149113.
89. Welch JLM, Hasegawa Y, McNulty NP, Gordon JI, Borisy GG. 2017. Spatial organization of a model 15-member human gut microbiota established in gnotobiotic mice. Proc Natl Acad Sci U S A 114:E9105–E9114. https://doi.org/10.1073/pnas.1711596114.
90. Gallego-Hernandez AL, DePas WH, Park JH, Teschler JK, Hartmann R, Jeckel H, Drescher K, Beyhan S, Newman DK, Yildiz FH. 2020. Upregulation of virulence genes promotes Vibrio cholerae biofilm hyperinfectivity. Proc Natl Acad Sci U S A 117:11010–11017. https://doi.org/10.1073/pnas.1916571117.
91. Caldara M, Friedlander RS, Kavanaugh NL, Aizenberg J, Foster KR, Ribbeck K. 2012. Mucin biopolymers prevent bacterial aggregation by retaining cells in the free-swimming state. Curr Biol 22:2325–2330. https://doi.org/10.1016/j.cub.2012.10.028.
92. Wheeler KM, Cárcamo-Oyarce G, Turner BS, Dellos-Nolan S, Co JY, Lehoux S, Cummings RD, Wozniak DJ, Ribbeck K. 2019. Mucin glycans attenuate the virulence of Pseudomonas aeruginosa in infection. Nat Microbiol 4:2146–2154. https://doi.org/10.1038/s41564-019-0581-8.
93. Shanks RMQ, Caiazza NC, Hinsa SM, Toutain CM, O'Toole GA. 2006. Saccharomyces cerevisiae-based molecular tool kit for manipulation of genes from Gram-negative bacteria. Appl Environ Microbiol 72:5027–5036. https://doi.org/10.1128/AEM.00682-06.
94. Barelle CJ, Manson CL, MacCallum DM, Odds FC, Gow NA, Brown AJ. 2004. GFP as a quantitative reporter of gene regulation in Candida albicans. Yeast 21:333–340. https://doi.org/10.1002/yea.1099.
95. Backer MDD, Maes D, Vandoninck S, Logghe M, Contreras R. 1999. Transformation of Candida albicans by electroporation. Yeast 15:1609−1618.

https://doi.org/10.1002/(sici)1097-0061(199911)15:15<1609::aid-yea485>3.3.co;2-p.
96. Ng JMK, Gitlin I, Stroock AD, Whitesides GM. 2002. Components for integrated poly(dimethylsiloxane) microfluidic systems. Electrophoresis 23:3461–3473. https://doi.org/10.1002/1522-2683(200210)23:20<3461::AID-ELPS3461>3.0.CO;2-8.
97. Holmén JM, Karlsson NG, Abdullah LH, Randell SH, Sheehan JK, Hansson GC, Davis CW. 2004. Mucins and their O-glycans from human bronchial epithelial cell cultures. Am J Physiol Lung Cell Mol Physiol 287:L824–L834. https://doi.org/10.1152/ajplung.00108.2004.
98. Sanders NN, Van Rompaey E, De Smedt SC, Demeester J. 2001. Structural alterations of gene complexes by cystic fibrosis sputum. Am J Respir Crit Care Med 164:486–493. https://doi.org/10.1164/ajrccm.164.3.2011041.
99. O'Toole GA. 2011. Microtiter dish biofilm formation assay. J Vis Exp 2011:2437. https://doi.org/10.3791/2437.
100. de Lorenzo V, Timmis KN. 1994. Analysis and construction of stable phenotypes in gram-negative bacteria with Tn5- and Tn10-derived minitransposons. Methods Enzymol 235:386–405. https://doi.org/10.1016/0076-6879(94)35157-0.